Hierarchization of USY Zeolite by NH_4OH. A post-synthetic process investigated by NMR and XRD.

Joost Van Aelst,[†] Mohamed Haouas,*[,‡] Elena Gobechiya,[†] Kristof Houthoofd,[†] An Philippaerts,[†] Sreeprasanth Pulinthanathu Sree,[†] Christine E. A. Kirschhock,[†] Pierre Jacobs,[†] Johan A. Martens,[†] Bert F. Sels,*[,†] Francis Taulelle[†,‡]

[†] *Centre for Surface Chemistry and Catalysis, KU Leuven, Kasteelpark Arenberg 23, Bus 2461, 3001 Heverlee, Belgium*

[‡] *Tectospin, Institut Lavoisier de Versailles, University of Versailles Saint Quentin en Yvelines, 45 avenue des Etats-Unis, 78035 Versailles Cedex, France*

* Corresponding author. MH : tel. +33 1 39 254 254; BS : tel. +32 16 32 15 93

E-mail address: mohamed.haouas@uvsq.fr, bert.sels@biw.kuleuven.be

Keywords: zeolite, hierarchical material, powder XRD, solid-state NMR, ^{29}Si MAS NMR, ^{27}Al MAS NMR, MQMAS, DQ-SQ, amorphization.

ABSTRACT :

Ammonia treatment of USY zeolite has led to a new hierarchical material. The local and global structural changes during the transformation have been monitored by XRD and by ^{1}H, ^{29}Si, and ^{27}Al solid-state NMR. A wealth of 1D and 2D NMR protocols were applied, including ^{1}H DQ-SQ, ^{27}Al MQMAS, ^{29}Si MAS and CPMAS as well as ^{1}H-^{29}Si HETCOR. The effects of aqueous ammonia treatment, different thermal post-treatments and rehydration were studied. An increasing loss of crystallinity was observed upon increasing duration of ammonia treatment. Under the experimental conditions a few percent of silica was lost into solution and no loss of aluminum was observed. But, increasing numbers of silanol groups were detected. The progressive transformation induces formation of mesopores, reduction of the fraction of the sample exhibiting Bragg crystallinity and apparition of a dense, amorphous aluminosilicate phase. The latter contains ammonium ions and strongly bound water which both are resistant to thermal decomposition up to 350°C. After about 24 hours of treatment the zeolite fraction has been completely transformed into the amorphous phase. At intermediate stages a complex hierarchical material is obtained with mesopores and zeolitic micropores next to the dense aluminosilicate, containing ammonium ions, highly structured water and silanols nests.

1. INTRODUCTION

Aluminosilicate zeolites are open framework solids that have been of great interest because of their potential use for catalysis, separation, and ionic exchange. Their unique physical and chemical properties such as ordered porosity determining their extended and reactive internal surface are at the origin of their particular catalytic and adsorption performances. Nevertheless, a handicap of today's zeolite technology is the mass-transfer restriction of guest species due to diffusion limitations. Significant research efforts have been devoted to the synthesis of ordered mesoporous materials, but in contrast to crystalline zeolites these materials found little application so far, because of the inherent amorphous nature of the walls separating the mesopores.[1] Rational structural design and synthesis methodology are vital for development of new classes of porous materials to overcome current challenges in the field of zeolite science.[2-4] To minimize diffusion problems various synthetic approaches have been developed, targeting for instance extra-large pore zeolites,[5,6] nanosized zeolite particles,[7,8] layered zeolite-nanosheets,[9-11] and hierarchical porous composites.[12-17] Post-synthesis modifications such as dealumination and desilication, have been found to be particularly convenient and efficient.[2,18-21]

Among these, treatment with bases was identified as powerful and elegant method preserving crystallinity and acidic properties of the parent zeolite, while mesoporosity was introduced.[22-25] Enhanced diffusion ability and improved catalytic performance have been proven in alkaline-mediated mesoporous zeolites.[26-31] However, the efficiency of mesopore formation was found to depend on the nature of the base and the structural type of the zeolite framework. Bases such as NH_4OH and Na_2CO_3 were shown to be less effective than NaOH.[30] Especially the preparation of hierarchical FAU

frameworks by exposure to base appeared challenging due to the sensitivity of the framework stability towards the Si/Al ratio.[32] Introduction of mesoporosity in zeolites of low framework density and low Al content, such as USY zeolites, needs particular precautions and mild conditions to avoid framework collapse.[33] Thorough structural, chemical, and textural characterization of the solids at each step of the post-synthesis protocol are essential to understand the transformation process. Such understanding could lead to improved post-synthesis treatments targeting the desired properties of the transformed materials. Solid-state nuclear magnetic resonance (NMR) and X-ray diffraction (XRD) are well-established tools for the characterization of zeolites and zeotype materials.[34-40] XRD quantifies the fraction of the materials exhibiting Bragg crystallinity, while ^{29}Si MAS NMR detects crystalline as well as amorphous non-framework material.[41] Recently, the creation of silanol nests, and hydroxyl nets associated to Al-OH in the framework of Y zeolite after alkaline treatment have been observed by using ^{27}Al{^{1}H} TRAPDOR experiments.[43] Moreover, healing of hydroxyl nests as a consequence of re-alumination during the treatment was proven by various NMR studies[43-45], although Lutz et al. did not observe a re-insertion of extra-framework Al into the zeolite framework.[42] During base post-synthetic treatment of zeolites silicon removal and aluminum insertion or migration, may occur together. Therefore simultaneous monitoring the effects these two processes have on structure and properties of the material is key to understand the global mechanism.

In the present study, a commercial de-aluminated Y sample (USY zeolite, CBV780 Zeolyst), was treated with aqueous ammonia to create a catalyst support with a hierarchical pore system containing micro- and meso-pores. The synthesis procedure and

benefits of the peculiar pore architecture for catalytic reactions with large reagents such as vegetable oils, has been described elsewhere.[46,47] The effect of contact time with the ammonia solution is investigated as well as the effect of subsequent thermal treatments. The crystallinity of the ammonia-treated samples is studied by powder XRD analysis, while extensive solid-state NMR complements the structural investigation of periodic and amorphous fraction of the materials. Particular attention is given to the nature of the amorphous phase and its evolution through the treatment with ammonium hydroxide.

2. EXPERIMENTAL SECTION

Sample Preparations. The parent material used in this study is a CBV780 USY zeolite (*Zeolyst International*, bulk Si/Al = 40, H-form). The solid (2.5 g) is added to an aqueous ammonia solution (0.02 M, 200 ml/g) and mechanically stirred at 250 rpm for 15 min – 24 h. Subsequently, the solution is immediately filtered and washed (3 times) with distilled water using a Büchner set-up and the retained solid is dried overnight either at ambient conditions (room temperature dried) or at 100 °C. To obtain the calcined form, the samples dried at 100 °C undergo a further programmed heat treatment in a U-tube oven under a nitrogen flow (2 $ml.s^{-1}.g^{-1}$). First, the sample is heated to 200 °C (2 °C/min; 30 min isothermal at 200 °C) and then the temperature is raised to 350 °C (3 °C/min; 30 min isothermal at 350 °C). To ensure a homogeneous gas flow through the powder, the zeolites were first pelletized to particle sizes in the range of 250 – 500 µm. The samples are denoted USY(*t*)-RT, USY(*t*)-100°C and USY(*t*)-calc for respectively the room temperature dried, 100 °C dried, and calcined base treated zeolites for a period of time *t* hours.

XRD Analyses. Powder XRD patterns were recorded at room temperature on a STOE STADI MP diffractometer with focusing Ge(111) monochromator ($CuK\alpha_1$ radiation, λ = 1.54056 Å) in Debye-Scherrer geometry with a linear position sensitive detector (PSD) with 6° 2θ window. Data were recorded in the 2θ range of 4 to 60.50° with a step width of 0.5°, internal PSD resolution 0.01°, and a counting time of 300 s per step. All samples were equilibrated above saturated NH_4Cl solution at relative humidity of 79% prior to the XRD measurement in order to ensure identical states of hydration. The crystalline, Bragg scattering fraction for all samples was obtained by least-squares fits of the intensity of the measured diffractograms by simulated XRD patterns over the whole measured data range. The intensity I(2θ) was simulated by weighed summation of crystalline ($I_c(2\theta)$) and amorphous ($I_a(2\theta)$) contributions. The former consisted of the set of the experimentally determined Bragg lines of the parent material and the latter of the experimental diffractogram of the non calcined sample treated for the longest time with ammonium hydroxide (24h) which exhibited only broad features.

$$I(2\theta) = \varepsilon_c.X_{c.}I_c(2\theta) + \varepsilon_a.(1- X_c).I_a(2\theta),$$

where X_c refers to the crystal fraction in the material, ε_c and ε_a to the mass absorption coefficient, which defines the probability scattering occurs at the respective phase. The crystalline fraction of each treated material was estimated in relation to the parent material whereof the crystal fraction was obtained from NMR analysis (see below and in Table 3). All XRD patterns were corrected for air and empty capillary scattering. The algorithm is implemented into the WinXPOW software (STOE & CIE GmbH 2009).

NMR Experiments. Spectra were measured at room temperature under magic angle spinning (MAS) conditions. The NMR spectra were obtained on a Bruker Avance-500 spectrometer equipped with a MAS accessory operating at 500.130, 130.320, and 99.351 MHz for ^{1}H, ^{27}Al, and ^{29}Si. A 4 mm zirconium oxide cylindrical-type rotor was used. The ^{1}H MAS Hahn echo spectra were recorded with an interpulse delay synchronized with the rotor period. Spectra were recorded with single 90° pulse for ^{29}Si (4.0 μs) or 15° pulse for ^{27}Al (0.5 μs), at a spinning rate of about 10 kHz for all nuclei. Repetition time was 1 s for ^{1}H, 215 s for ^{29}Si and 0.1 s for ^{27}Al. High power decoupling with ^{1}H rf strength of ca. 42 kHz was applied in the case of ^{29}Si. The chemical shifts were calibrated relative to external standards, tetramethylsilane for ^{1}H and ^{29}Si and 1 M aqueous $Al(NO_3)_3$ for ^{27}Al (set to $\delta = 0$ ppm in each case).

The ^{1}H–^{1}H DQ–SQ MAS correlation spectra were obtained using the POSTC7 sequence with excitation and conversion periods of 0.2 ms. The two-dimensional spectra were collected with 128 t_1 increments of 200 μs and 16 transients each using the hypercomplex quadrature detection in the indirect dimension.

The ^{1}H→^{29}Si CPMAS and ^{1}H→^{29}Si HETCOR NMR spectra were run with RF field ca. 63 kHz and 73 kHz for ^{29}Si and ^{1}H respectively, and 10 ms contact time. ^{1}H SPINAL-64 decoupling was applied during the ^{29}Si signal acquisition (pulse length 12.0 μs, RF field ca. 42 kHz). 54 t_1 slices with 1024 transients each were recorded for the 2D experiment.

The ^{27}Al multiple-quantum MAS[48] (MQMAS) NMR spectra were recorded using the three-pulse z-filter sequence, a single continuous-wave pulse for excitation of triple quantum (3Q) coherences, and the FAM II sequence for 3Q→0Q conversion. A 2-D

Fourier transformation followed by a shearing transformation yielded pure absorption 2D NMR spectra.

For dehydrated samples, a specific homemade device was used to evacuate the sample and seal the 4 mm NMR rotor without exposure to ambient atmosphere prior to each NMR experiment. Around 80 mg of the powder zeolite was first treated at 250 °C/2 days and subsequently outgassed at room temperature for 3 h (< 10^{-7} mbar). The weight-loss observed upon dehydration was about 20%. All samples are spontaneously re-equilibrated with water in ambient air for few days unless specified differently.

3. RESULTS AND DISCUSSION

It is well established that treatment with a basic solution can affect the crystallinity of zeolites. The extent of crystal fraction loss obviously depends on the alkalinity of the solution, the treatment time, and the pristine parent zeolite (i.e. its framework Si/Al ratio). The powder XRD patterns of calcined samples are shown in Figure 1. A continuous intensity decrease and broadening of Bragg diffraction peaks with contact time is observed. The overall XRD results in determination of a crystal fraction are summarized in Table 1. The next sections will provide insight on the local structural changes occurring during the transformation as sensed by solid state NMR spectroscopy.

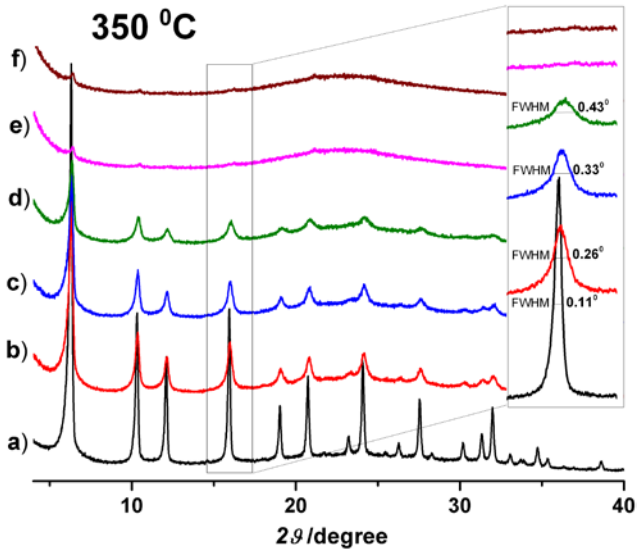

Figure 1. XRD patterns of USY samples before (a) and after NH_4OH treatment at different contact times and subsequently dried at 100 °C followed by calcination at 350 °C (b-f): a) pristine zeolite, b) USY(0.25)-calc, c) USY(1)-calc, d) USY(5)-calc, e) USY(16)-calc, f) USY(24)-calc. In the inset a broadening of the diffraction peak at ~16° 2θ is displayed, indicated by the full width at half height.

Table 1. Crystal fraction in Calcined USY Zeolites Treated with NH_4OH Solution at Different Reaction Times, Measured by XRD. *

Contact time (h)	Calcined at 350 °C
0	59.0
0.25	41.3
1	35.4
5	22.4

16	4.1
24	2.4

***** The given numbers have been normalized to the value of crystalline fraction in the pristine material obtained from NMR.

Influence of Ammonia Treatment Time. The samples studied in this section are those calcined at 350 °C (USY(*t*)-calc). The multinuclear NMR analyses are conducted in both the hydrated state and after dehydration.

The ^{1}H MAS NMR spectra of samples in hydrated state are dominated by a signal of water around 4.5-4.6 ppm (see Supporting Information Figure S1). This resonance corresponds to physisorbed water moving freely in the pore system of the zeolite. A broader line is observed after longer NH_4OH treatment, i.e. 16 and 24 h. This is due to slowed dynamic exchange of water molecules. One expects increasing structural loss upon increasing treatment time. Magnification of the spectra allows to distinguish some small resonances in the range 0-2 ppm, which can be assigned to isolated silanol groups and/or Al-OH species (see Figure S2). Also, a distinct signal around 6.8 ppm is visible due to ammonium cations as indicated by the partially resolved triplet feature caused by the scalar coupling $^{1}J(^{1}\text{H}\text{-}^{14}\text{N})$. This signal only occurs in the base treated samples confirming that the ammonium species stem from the base solution. Furthermore, the presence of this signal in these spectra even after calcination indicates that these ammonium species are strongly stabilized either trapped in closed pores or strongly hydrogen-bonded to the surroundings.

Beside this resonance, the spectra of dehydrated samples (Figure 2) exhibit a composite resonance around 1.6-1.8 ppm due to terminal silanol groups, and a broad

shoulder in the range 2.0-3.5 ppm, assigned to water molecules hydrogen-bonded to silanols.[35] Like ammonium ions, these residual water molecules also interact strongly with their surroundings (vide infra). Spectral decomposition allows quantification of each of these species (Table 2). Ammonium ions as well as water molecules remaining in the compound increase with treatment time, as a consequence of Si-O-Si hydrolysis. Additionally, a slight increase of terminal silanol groups with treatment time is observed. When dehydrated samples were subjected to progressive rehydration, the resonances of water and of silanols broadened as a consequence of increasing chemical exchange. During the process a resonance at ca. 1.1 ppm appears (see Supporting Information Figure S3). This resonance very weakly occurred in the parent material and was then assigned to some residual amounts of extra-framework aluminum resulting from the incomplete elimination of extra-framework aluminum (EFAL) from USY after acidic treatment. However, in the ammonia treated samples this signal has been identified as Al-OH-Al bridging hydroxide formed upon hydration.[51] The hydration state also affected the ammonium resonance. Dehydration led to a slight up-field shift (from 6.9 to 6.5 ppm), reversible upon dehydration-rehydration cycles. Ammonium ions are therefore accessible to water molecules.

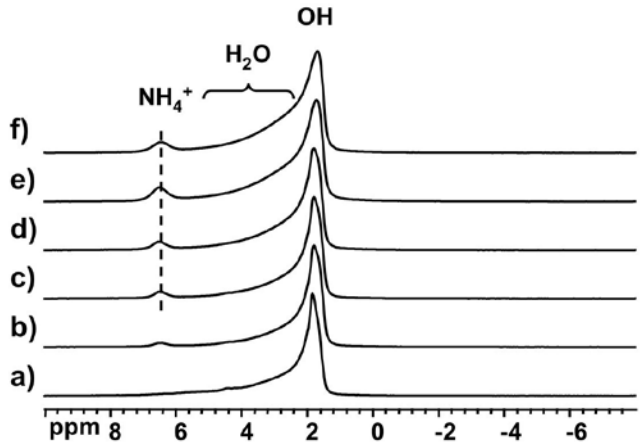

Figure 2. Stack plot of ^{1}H MAS NMR spectra of dehydrated USY samples before and after treatment with NH_4OH solution for different contact times and subsequently dried at 100 °C followed by calcination at 350 °C: a) pristine zeolite, b) USY(0.25)-calc, c) USY(1)-calc, d) USY(5)-calc, e) USY(16)-calc, f) USY(24)-calc.

Table 2. Amounts (mmol/g) of Protonated Species as Determined by ^{1}H MAS NMR in Dehydrated Calcined USY Zeolites Treated with NH_4OH Solution at Different Reaction Times.

Sample	NH_4	H_2O	OH
	6.5 ppm	2.0-3.5 ppm	1.6-1.8 ppm
Pristine	0.00	0.80	0.59
USY(0.25)-calc	0.03	1.49	0.86
USY(1)-calc	0.05	1.48	0.84
USY(5)-calc	0.05	1.38	0.84
USY(16)-calc	0.09	1.61	1.02
USY(24)-calc	0.07	1.44	0.93

To gain more insight on proximity and mutual interaction between proton species, 2D correlation NMR experiments were performed. Figure 3 shows an example of 2D DQ-SQ ^{1}H-^{1}H POST-C7 spectrum obtained on the dehydrated sample of 16 h treated zeolite (USY(16)-calc). The spectrum exhibits a strong autocorrelation for terminal silanol resonance at 1.8 ppm, indicating silanol nests. No autocorrelation neither for the broad water distribution nor for ammonium ion resonances are observed. Water resonances display a specific pattern of pairs of distinct resonances indicating that the two hydrogen atoms of each water molecule are inequivalent. Such a situation is consistent with asymmetric hydrogen bonding for all water molecules. Neither motion nor chemical exchange average their chemical shift indicating very strong water clustering within the silanols nests. Ammonium resonances do not exhibit any autocorrelation in the DQ-SQ spectrum, but exhibit coupling to all water and silanol resonances. One can therefore deduce that still some local tetrahedral reorientation of ammonium ions takes place, even at frequencies as low as a millisecond. This averages out the dipolar coupling between proton and NH_4^+, but does not average the dipolar coupling between ammonium protons, water and silanol protons. As these clusters are located close to the regions where most Si-O-Si are broken, they are most probably situated at the inner surface of the mesopores created by ammonia treatment.

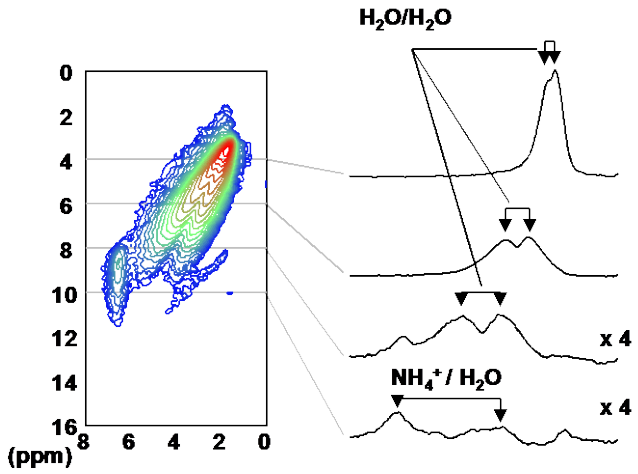

Figure 3. 2D DQ-SQ ^{1}H-^{1}H POST-C7 spectrum of the dehydrated sample treated with NH_4OH solution for 16 h (USY(16)-calc). Somme selected slices along the t_1 axis are shown.

Figure 4 shows the ^{29}Si MAS NMR spectra of USY samples before and after NH_4OH treatment for different contact times recorded in single pulse mode. The spectra exhibit a set of broad signals centered at ca. -112, -101, and -91 ppm assigned to silicon with Q^4, Q^3, and Q^2 environment, respectively. The relatively sharp line at ca. -107 ppm is due to Q^4 silicon sites in a well ordered zeolite Y framework.

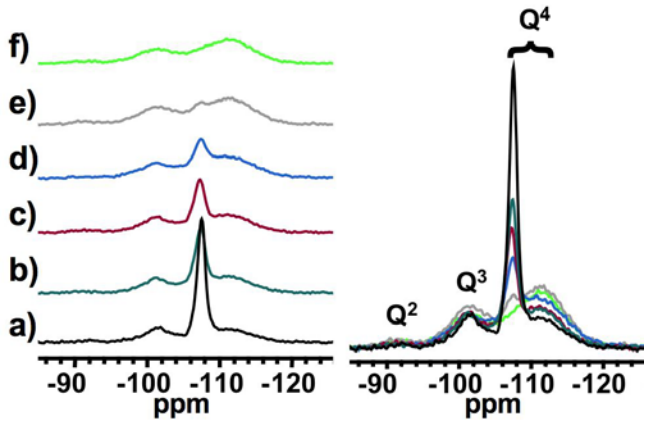

Figure 4. Stack plot (left) and superimposed (right) of ^{29}Si high power decoupled MAS NMR spectra of USY samples before and after treatment with NH_4OH solution for different contact times and subsequently dried at 100 °C followed by calcination at 350 °C: a) pristine zeolite, b) USY(0.25)-calc, c) USY(1)-calc, d) USY(5)-calc, e) USY(16)-calc, f) USY(24)-calc.

A quantitative spectral decomposition (an example is shown in Figure S4) allows an estimate of the amounts of each component (Table 3). In line with the progressive decrease of crystalline fraction with the increasing duration of ammonia treatment, the area of the resonance due to the framework zeolite drops from 59% to 6% of total Si, after 24 h of treatment. In Figure S5, the correlation of quantification between XRD and NMR methods for USY, is displayed. XRD and NMR both consistently estimate the crystal fraction of samples studied, by two different ways: measuring integrity of bonding by NMR or integrity of the periodic framework by XRD.

It is worth noting that a significant fraction of amorphous siliceous material was present already in the parent USY zeolite. Most probably this fraction resulted from the post-synthetic steaming treatment to stabilize the USY framework. Quantitative comparison of the spectra of ammonia treated samples with the spectrum of the parent zeolite, revealed a global signal loss of 9-13% after exposure to NH_4OH for 1-24 h. Interestingly, the maximum amount of silicon in the supernatant is reached already after 1 h of treatment, indicating the limited solubility of silica in these conditions. However, the fraction of silica found in the liquid phase not necessarily corresponds to the occurring framework desilication. Indeed, after 1 h of treatment, the fraction of crystalline material continued

to decrease, while the fraction of disordered solid material increased simultaneously. This amorphous material resulting from framework breakdown therefore remained in the solid fraction. According to NMR this amorphous material showed high condensation state since the ammonia treatment mainly generated non-periodic Q^4 Si species whereas the Q^3 Si fraction did not alter significantly. However, for prolonged treatment times the fraction of Q^2 species also substantially increased, most probably as a consequence of defect formation.

Table 3. Fraction (%) of Q^n Si Population as Determined by ^{29}Si hpDec MAS NMR in Calcined USY Zeolites Treated with NH_4OH Solution at Different Reaction Times.

Sample	^{4}Q	^{3}Q	^{2}Q	^{4}Q	Total Si observed
		disordered		USY	
pristine	19	21	1	59	100
USY(0.25)-calc	31	23	1	42	96
USY(1)-calc	32	26	2	32	91
USY(5)-calc	46	22	1	18	87
USY(16)-calc	50	32	3	7	91
USY(24)-calc	53	24	4	6	87

^{29}Si CPMAS NMR shows the same broad signals at ca. -112, -101, and -91 ppm together with the parent framework resonance at -108 ppm, but their relative proportions are altered considerably, as proximity to protons in the vicinity affects the signal

intensity. The resonance due to the framework zeolite appeared very weak as a result of moderate CP transfer efficiency because in the undisturbed Q^4 network only few defects are present. This resonance contrasts with the more efficient CP transfer for Q^4 species in the previously identified amorphous phase. Clearly some silanols in vicinity to these Q4 sites are present. The dominant resonance, however, originates from Q^3 species (75-80%), followed by that of Q^4 (15-20%) and the signal of Q^2 (5-10%), the latter now being clearly visible in CPMAS acquisition mode. This is consistent with the existence of H-Si dipolar interaction due to the presence of silanols in these Si sites. The Q^3 resonance appears as a composite of a narrow and broad signal at the same position. With longer treatment times the broad component increasingly grew at the expense of the narrow one. A slightly higher CP efficiency is observed with dehydrated samples due to reduced mobility of protonated species after evacuation of physisorbed water molecules. Figure 5 shows the CPMAS spectra obtained on the series of dehydrated samples. The global signal intensity increases with ammonia treatment time, by a factor of ca. 1.6 compared to the parent material for samples treated for 5-24 hours. The $^{29}Si\{^1H\}$ CPHETCOR experiments (Figure S6) on both hydrated and dehydrated samples showed that all protonated species present in the solid participate in the CP transfer to the ^{29}Si nuclei including silanol, ammonium ions and water molecules. Considering the relatively long contact time (10 ms) spin diffusion takes place and the CP dynamics is governed by the protons spin bath of all ammonium ions and water molecules in strong interaction with the framework. This clearly confirms the earlier observation that a dense, amorphous silicate phase is formed at the expense of the crystalline zeolite structure.

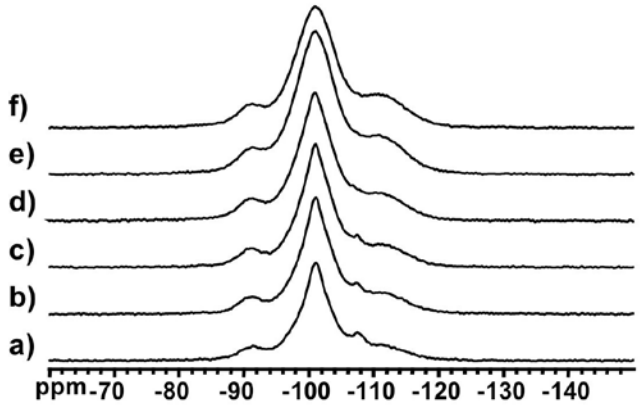

Figure 5. Stack plot of ^{29}Si CPMAS NMR spectra of dehydrated USY samples before and after treatment with NH_4OH solution for different contact times and subsequently dried at 100 °C followed by calcination at 350 °C: a) pristine zeolite, b) USY(0.25)-calc, c) USY(1)-calc, d) USY(5)-calc, e) USY(16)-calc, f) USY(24)-calc.

^{27}Al MAS NMR spectra of the parent and the early stages of exposure to exhibit two resonances (Figure 6). A dominant resonance at 63 ppm, corresponding to tetrahedrally coordinated aluminum in the intact USY and a small resonance at 0 ppm, (less than 5%), related to some extra-framework aluminum atoms (EFAL) respectively.[33,42,44,45] With prolonged NH_4OH treatment the spectra evolution reveals a correlated decrease of the 63 ppm resonance to growth of a resonance at 57 ppm. The small amount of hexacoordinated EFAL disappears progressively with time of treatment. The decrease of the framework USY ^{27}Al resonance follows the same trend of its equivalent ^{29}Si resonance at -108 ppm shown in Figure 4. The overall amount of Al in the sample did not significantly change, which indicated, as expected, that no significant dealumination took place during ammonia treatment.

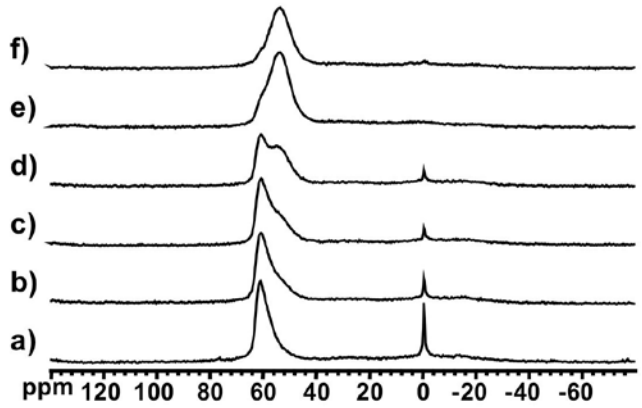

Figure 6. Stack plot of ^{27}Al MAS NMR spectra of USY samples before and after treatment with NH_4OH solution for different contact times and subsequently dried at 100 °C followed by calcination at 350 °C: a) pristine zeolite, b) USY(0.25)-calc, c) USY(1)-calc, d) USY(5)-calc, e) USY(16)-calc, f) USY(24)-calc.

MQMAS experiments were acquired to provide insight into the evolution of local order of aluminum atoms during exposure of USY to ammonia.[52,53] Figure 7 compares 2D sheared ^{27}Al MQMAS NMR spectra of the parent zeolite with samples after treatment. The spectrum of the parent USY (Figure 7a) displays a well-defined resonance at 63 ppm, typical for USY in a highly crystalline state. Already after 0.25 h treatment time, the ^{27}Al MQMAS spectrum shows the additional resonance already observed in the 1D MAS spectrum (Figure 6b and Figure 7b). Monitoring furthering of evolution with time of ammonia treatment is shown in Figure 7c to f). With increasing treatment time this signal gains intensity at the expense of the sharp signal indicating the progressive conversion of the ordered phase into a less crystalline state. The spread of the resulting cross peak along the diagonal ($\delta_{iso} = \delta_{F2}$) in the 2D MQMAS spectra clearly indicates a large distribution of isotropic chemical shifts as well as a small distribution of $C_{QCC,}$ the

quadrupolar coupling constant. The isotropic shift range from 55 to 57 ppm has C_{QCC} values of ca. 2.4-2.7 MHz, which are very close to those of the sharp signal of the ordered phase, i.e., 2.2-2.6 MHz. This suggests that the aluminum sites in the disordered phase still preserve the characteristic tetrahedral coordination, known from the zeolite framework. The chemical shift distribution most probably arises from a newly created distribution of Al-O bond distances and Si-O-Al bond angles, indicating a loss of periodicity. On the other hand, the rather limited distribution of C_{QCC} could be explained from the dominant contribution of the local p-orbital term to the C_{QCC}, compared to the long distance point charge distribution in a lattice. The latter also can be assumed to be at least partially averaged by fluctuating water molecules in the spontaneously rehydrated samples. Already the spectrum of the parent zeolite shows traces of this broad component, which indicates an amorphous phase in very low amounts already was present. Most probably these traces arose from the dealumination/steaming treatment of USY and is consistent with the ^{29}Si NMR results.

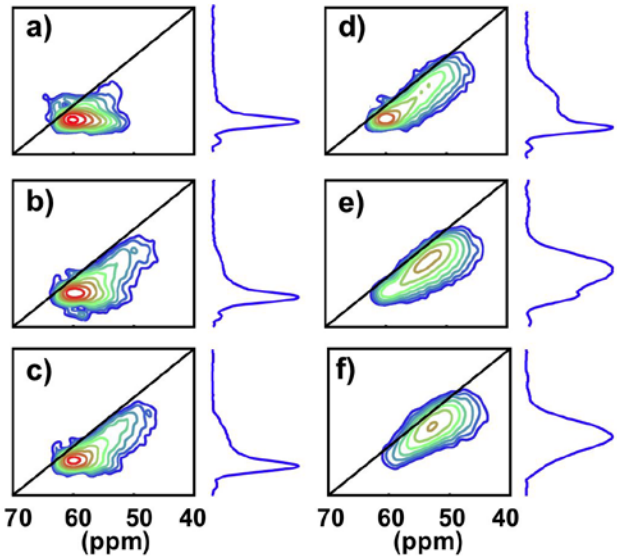

Figure 7. ^{27}Al MQMAS NMR spectra of USY samples before and after NH_4OH treatment for different contact times and subsequently dried at 100 °C followed by calcination at 350 °C: a) pristine parent zeolite, b) USY(0.25)-calc, c) USY(1)-calc, d) USY(5)-calc, e) USY(16)-calc, f) USY(24)-calc. The sheared spectra are displayed as contour plots. The projection along the F1 axis is the isotropic dimension.

The identical but dehydrated samples have also been measured by ^{27}Al MAS NMR. The spectra are shown in the Supporting Information (Figure S7). Dramatic signal broadening is observed for all resonances leading to a significant fraction of "NMR silent" quadrupolar species. The extent of broadening strongly depended on the resonance. The signals originating from tetracoordinated aluminum atoms of the crystalline zeolite framework experienced a very large C_{QCC} up to 9 MHz and only 10% of its original signal area could be measured, whereas the width of the resonance of aluminum in the disordered materials was less affected by dehydration and almost the totality of its original signal area was quantitatively observed. This strong contrast between hydrated and dehydrated state is driven by the water mobility in the zeolite framework, which is averaging out the quadrupolar interactions. The observation that the disordered phase is much less affected clearly indicates that in this phase the water molecules are still close enough and interacting with aluminum atoms without too much fluctuation in position.

Influence of Thermal Treatment on Ammonia Treated Samples. In this section the effect of thermal treatment subsequent to NH_4OH exposure for 0.25, 5, and 24 h is presented. Powder XRD patterns of room temperature dried, 100°C dried and

calcined samples are shown in Figure S10. Thermal post-treatment influences the crystalline fraction of the eventually measured sample. This fraction is obviously larger for the 100 °C dried and calcined samples. As-obtained samples (dried at room temperature) contain water and ammonium hydroxide. Thermal post-treatments remove physically adsorbed water from the samples. Aging of as-obtained samples without thermal treatment stage, leads to a progressive decrease of crystal fraction with time by mobile water assisted hydrolysis. Drying at 100°C and subsequent calcination respectively slows down and quenches this evolution (Figure S9). To monitor the impact of NH_4OH treatment time, immediate drying at elevated temperature and calcination must be performed at the end of treatment, followed by subsequent XRD or NMR crystal fraction measurement. In Figure 8 ^1H NMR spectra for samples without thermal treatment, after100 °C drying and after calcination at 350 °C are shown. Most spectra contain a resonance of water at 4.1-4.8 ppm depending on the hydrophobicity of the sample. Magnification of the spectra (Figure 8), allowed identification of the ammonium cation resonance, mainly in spectra of calcined materials. Ammonium ions in non-calcined samples are in chemical exchange with mobile water, while ammonium ions in calcined samples are trapped in the disordered phase, allowing their observation. Rehydration of the calcined samples is a slow process, not completed even after few weeks (Figure S3). One can observe from ^1H NMR even after calcination, not all water is removed from the samples. Strongly bound water in the amorphous phase is present, as visible in Figure 3. Ammonium ions are embedded in such water clusters as the 2D DQ-SQ ^1H-^1H spectrum (Figure 3) shows. Ammonium species are part of structured and rigid H-bond clusters with water and hydroxyl groups. They were not completely decomposed

by the reasonably mild calcination conditions selected. It is worth noting that the non-crystalline structuring and densification could only be reliably observed after calcination.

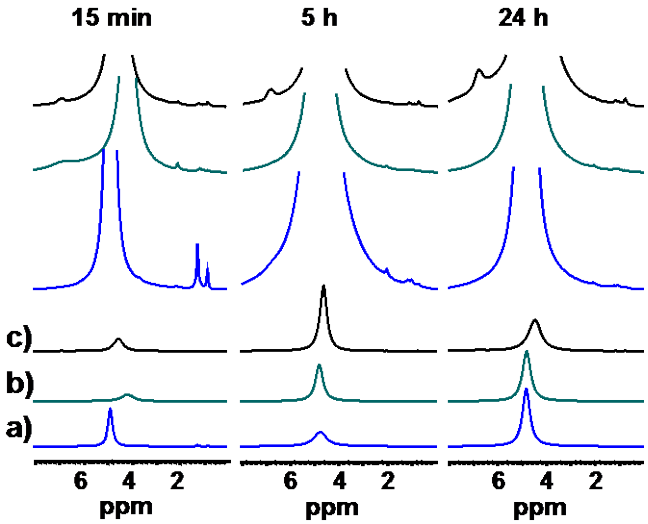

Figure 8. ^{1}H MAS NMR spectra of USY samples after NH_4OH treatment for 0.25, 5, and 24 h and subsequently a) dried at room temperature (USY(0.25)-RT, USY(5)-RT, and USY(24)-RT), b) dried at 100 °C (USY(0.25)-100°C, USY(5)-100°C , and USY(24)-100°C), and c) dried at 100 °C followed by calcination at 350 °C (USY(0.25)-calc, USY(5)-calc, and USY(24)-calc). On top, vertical expansions are displayed.

^{29}Si CPMAS spectra shown in Supporting Information (Figure S8) highlight mainly resonances of disordered phase (^{4}Q) as well as defect sites (^{2}Q and ^{3}Q). The efficiency of the CP transfer (gain in magnetization) is more effective in thermally treated materials, by reducing mobility of protons (silanols and water). Likewise ^{27}Al MAS spectra (Figure 9) show no crystalline phase in ^{27}Al spectra in samples treated for 5 h and 24 h without calcination at 350 °C. However, for 15 min treated samples the characteristic zeolitic aluminum resonance at 63 ppm is also observed in non-calcined

samples. For the calcined samples, this resonance exhibits an area of 93%, 40% and 15% of the original parent resonance area for samples treated for 0.25, 5 and 24 h respectively. For the sample treated for 15 min, this resonance area increases with temperature of the thermal post-treatment from 44% to 73% to 93% of the original parent resonance area for room temperature, 100 °C and 350 °C treated samples, respectively. This can be attributed to the progressive degradation of the zeolite crystal in non-calcined samples after synthesis. Also, a weak small sharp signal at 0 ppm is observed in the calcined samples, indicating the presence of some, though very few, extra-framework Al species (< 2%).

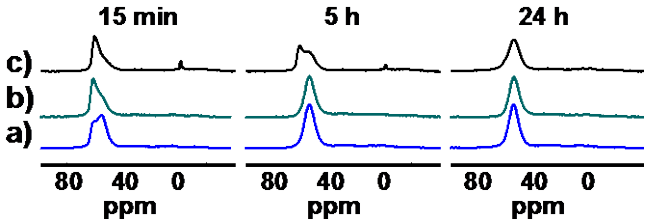

Figure 9. ^{27}Al MAS NMR spectra of USY samples after NH_4OH treatment for 0.25, 5, and 24 h and subsequently a) dried at room temperature (USY(0.25)-RT, USY(5)-RT, and USY(24)-RT), b) dried at 100 °C (USY(0.25)-100°C , USY(5)-100°C , and USY(24)-100°C), and c) dried at 100 °C followed by calcination at 350 °C (USY(0.25)-calc, USY(5)-calc, and USY(24)-calc).

In full agreement to these observations ^{29}Si MAS NMR spectra recorded under direct polarization (Figure 10), showed the characteristic feature of the ordered phase at -107 ppm for only 15 min treated sample before thermal treatment accounting of 32% of the original parent resonance area (Figure 10a). After drying at 100 °C (Figure 10b) this

resonance amounts to 62% for sample treated 15 min, but only ca. 1% and less than 1% in samples treated for 5, and 24 h, respectively. Calcination at 350 °C (Figure 10c) resulted in higher relative crystal fractions of 71%, 31% and 11%.

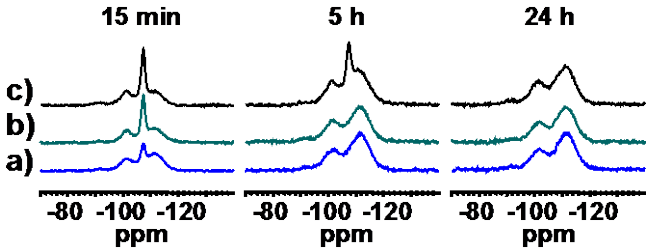

Figure 10. ^{29}Si MAS NMR spectra of USY samples after NH_4OH treatment for 0.25, 5, and 24 h and subsequently a) dried at room temperature (USY(0.25)-RT, USY(5)-RT, and USY(24)-RT), b) dried at 100 °C (USY(0.25)-100°C , USY(5)-100°C , and USY(24)-100°C), and c) dried at 100 °C followed by calcination at 350 °C (USY(0.25)-calc, USY(5)-calc, and USY(24)-calc).

The crystal fraction measured by XRD as well as with NMR after calcination may differ from the values obtained for room temperature and 100 °C dried samples. Actually, room temperature drying procedure does not quench the role of NH_4OH introduced into USY. Hydroxide treatment acts on opening Si-O-Si and Al-O-Si bonds with water assistance. After filtration and washing of the powder, some remaining hydroxides are probably present, slowly keeping breaking bonds in the presence of mobile water. Depending on the drying/calcination procedure, the amount of mobile water left inside and thus the susceptibility towards ongoing bond breaking differs (see Figures 9, 10, S9 & S10). When room temperature drying occurs, it takes a few hours to eliminate the adsorbed water, leaving room for migration of hydroxide along the network, keeping

breaking bonds (see Figures 9, 10, S9 & S10). Furthermore, the determined crystal fraction for non-stable samples depends on the time spent with an excess of water hydrated state. Rehydration for standard XRD measurements, also adds to crystal network degradation. Therefore, only immediate drying, preferably quickly followed by calcination, and no delayed measurements can be reliably used to monitor the sample state evolution.

The Local Structure of the Base Modified Zeolite. When treating a zeolite with alkaline base, it is usually assumed that desilication occurs. In this specific situation of ammonia treatment at low concentration, very low level of desilication takes place.

By ^{1}H NMR, SQ and 2D DQ-SQ it has been shown that silanol nest are present in the dry amorphous phase, and strongly bound water crystallizes inside this phase in proximity to silanol nests and ammonium ions. ^{29}Si MAS demonstrated that by NH_4OH treatment a migration of Q^4 sites from the zeolite to the non-crystalline phase takes place. According to ^{29}Si CPMAS the efficiency of the polarization transfer increases by a factor of about 1.6 for the non-crystalline phase compared to the parent zeolite. Therefore distances between protons and Si atoms are shorter and the number of protons participating to the transfer is larger, typical for a dense phase, when compared to the parent zeolite. ^{27}Al MAS and MQMAS showed that aluminum atoms follow the same trend as silicon atoms. They migrate from q^4, i.e., $Al(OSi)_4$ environment, in the zeolite to q^4 in the non-crystalline phase. MQMAS confirms this evolution as the transition of a well defined crystallographic site to a tetrahedral site in a non-crystalline phase with a

chemical shift distribution typical for a network with low degree of ordering.

The picture of the transformation can now be established (Figure 11). Ammonia treatment slowly breaks Si-O-Si bonds of the zeolite, leaving a partially defective zeolite network. The remaining crystal fraction decrease with the length of exposition time to NH_4OH solution. Some islands of isolated silicate remain dispersed in the zeolite framework and irreversibly form a dense phase containing strongly bound ammonium ions and water molecules. This shrinking of zeolite fragments into a dense phase increases the volume and number of the mesopores, while decreasing the micropore volume. After long exposure times to ammonia solution, the end of the transformation, no significant observable zeolite phase is left, and the hierarchical material mainly consists of mesopores, surrounded by a dense hydrated ammonium silicate. The latter is resistant to heating, for the contained ammonium ions and water molecules are not removed by calcination.

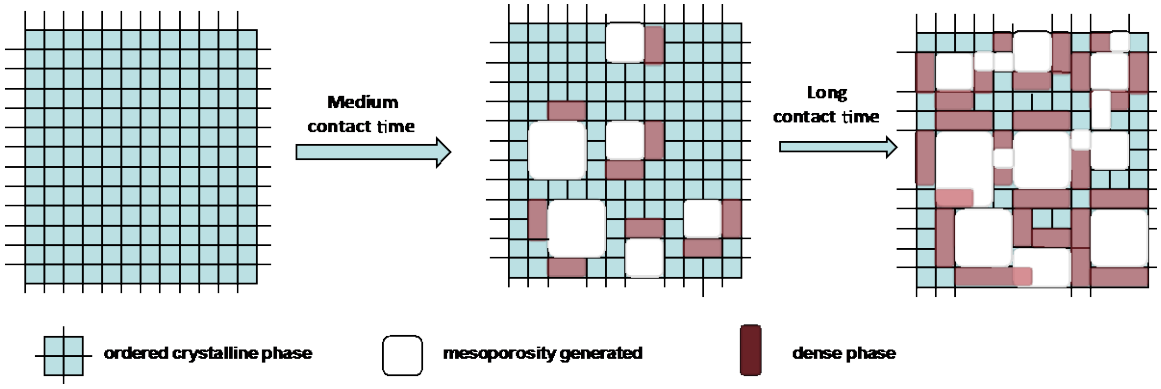

Figure 11. Schematic drawing of hierarchization with mesoporous carving and progressive amorphization at the surface of mesopores. Calcination allows quenching of NH_4OH bond breaking by water elimination, structural annealing of the dense amorphous phase and consolidation of the hierarchical material.

A schematic representation of the amorphous hydrated ammonium silicate is sketched in Figure 12. The bridging hydroxyl groups would be the preferential interaction sites between the ammonium hydroxide and the surface involving acid-base protonic transfer. A concerted reaction between ammonium hydroxide and the acidic site Al-OH-Si silicates leads to a bond breaking of Al-(OH)Si with correlated $AlOH\text{-}HNH_3$ and SiOH formation. This reaction is therefore accompanied by hydration of ammonium ion producing water nests including ammonium ions.

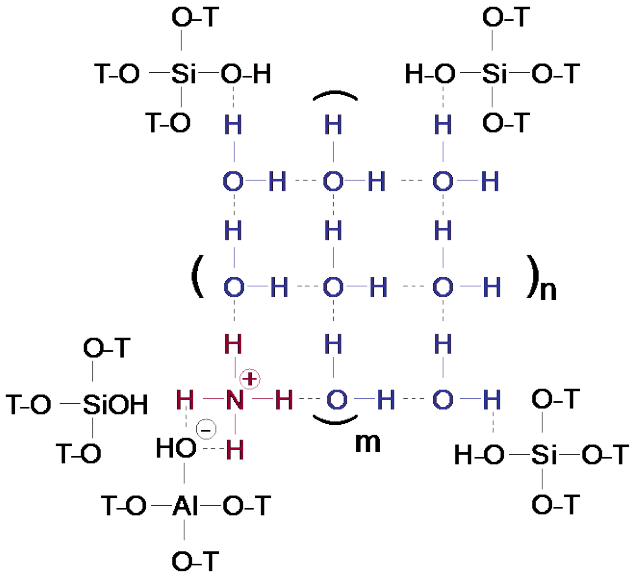

Figure 12. Proposed local structuration of the amorphous hydrated ammonium silicate phase.

4. CONCLUSION

Alkaline treatment of zeolite is known to lead to desilication. Creation of hierarchical materials is often associated to generating mesopores, insuring the facile diffusion of molecules to reach the micropores where the acid sites are located.

The ammonia treatment of a commercial CBV780 USY zeolite from *Zeolyst International* exhibiting a bulk Si/Al ratio of 40 under H-form, to generate mesoporosity as earlier reported,[46] led to a very moderate desilication accompanied by a dramatic loss in crystallinity. Hierarchical materials generation was sought through basic treatment of zeolites, with an additional calcination step. This process leads to large meso-sized pores with transformation of the initial zeolitic network into a dense hydrated ammonium silicate amorphous phase.

The process of preparing a hierarchical material by NH_4OH treatment of USY followed by thermal treatment of the material was studied by XRD and solid state NMR with a large set of experiments of ^{1}H, 1D SQ, 2D DQ-SQ, ^{29}Si MAS, CPMAS, and ^{27}Al MAS, MQMAS, ^{1}H-^{29}Si HETCOR. A variety of progressive steps of NH_4OH treatment followed by different thermal treatments and different dehydration and rehydration schemes were monitored. The obtained results demonstrate a stunningly clear picture of the process at the atomic level. With this NH_4OH treatment it has been clearly shown that the transformation involves the conversion of a crystalline zeolite network

into a dense amorphous phase, leading to increase of the total mesoporosity volume resulting into a new hierarchical material.

ACKNOWLEDGEMENTS

Research funded by a Ph.D. grant (J.V.A.) of the Agency for Innovation by Science and Technology (IWT). A.P. acknowledges F.W.O.-Vlaanderen (Research Foundation – Flanders) for a postdoctoral fellowship. B.F.S. and A.P. also thank the KU Leuven for financial support with the framework of Industrial Research Foundation (IOF). F.T. acknowledges KU Leuven for an appointment as visiting professor. E.G. and C.E.A.K. acknowledge the Belgian Prodex Office and ESA for financial support. This work was supported by long-term structural funding by the Flemish Government (Methusalem) and Belgian IAP-PAI networking.

REFERENCES

(1) Bein, T. *Stud. Surf. Sci. Catal.* **2007**, *170*, 41-53.
(2) Perez-Ramirez, J.; Christensen, C. H.; Egeblad, K.; Groen, J. C. *Chem. Soc. Rev.* **2008**, *37*, 2530-2542.
(3) Coronas, J. *Chem. Eng. J.* **2010**, *156*, 236-242.
(4) Serrano, D. P.; Escola, J. M.; Pizarro, P. *Chem. Soc. Rev.* **2013**, *42*, 4004-4035.
(5) Corma, A.; Diaz-Cabanas, M. J.; Jorda, J. L.; Martinez, C.; Moliner, M. *Nature* **2006**, *443*, 842-845.
(6) Gao, F. F.; Jaber, M.; Bozhilov, K.; Vicente, A.; Fernandez, C.; Valtchev, V. *J. Am. Chem. Soc.* **2009**, *131*, 16580-16586.
(7) Cundy, C. S.; Cox, P. A. *Microporous Mesoporous Mat.* **2005**, *82*, 1-78.
(8) Majano, G.; Mintova, S.; Ovsitser, O.; Mihailova, B.; Bein, T. *Microporous Mesoporous Mat.* **2005**, *80*, 227-235.
(9) Choi, M.; Na, K.; Kim, J.; Sakamoto, Y.; Terasaki, O.; Ryoo, R. *Nature* **2009**, *461*, 246-U120.

(10) Liu, Z.; Fujita, N.; Miyasaka, K.; Han, L.; Stevens, S. M.; Suga, M.; Asahina, S.; Slater, B.; Xiao, C. H.; Sakamoto, Y.; Anderson, M. W.; Ryoo, R.; Terasaki, O. *J. Electron Microsc.* **2013**, *62*, 109-146.
(11) Bleken, B. T. L.; Wragg, D. S.; Arstad, B.; Gunnaes, A. E.; Mouzon, J.; Helveg, S.; Lundegaard, L. F.; Beato, P.; Bordiga, S.; Olsbye, U.; Svelle, S.; Lillerud, K. P. *Top. Catal.* **2013**, *56*, 558-566.
(12) Kirschhock, C. E. A.; Kremer, S. P. B.; Vermant, J.; Van Tendeloo, G.; Jacobs, P. A.; Martens, J. A. *Chem.-Eur. J.* **2005**, *11*, 4306-4313.
(13) Snyder, M. A.; Tsapatsis, M. *Angew. Chem.-Int. Edit.* **2007**, *46*, 7560-7573.
(14) Zhu, Y.; Hua, Z. L.; Zhou, J.; Wang, L. J.; Zhao, J. J.; Gong, Y.; Wu, W.; Ruan, M. L.; Shi, J. L. *Chem.-Eur. J.* **2011**, *17*, 14618-14627.
(15) Zhao, J. J.; Hua, Z. L.; Liu, Z. C.; Li, Y. S.; Guo, L. M.; Bu, W. B.; Cui, X. Z.; Ruan, M. L.; Chen, H. R.; Shi, J. L. *Chem. Commun.* **2009**, 7578-7580.
(16) Zhou, J. A.; Hua, Z. L.; Zhao, J. J.; Gao, Z.; Zeng, S. Z.; Shi, J. L. *J. Mater. Chem.* **2010**, *20*, 6764-6771.
(17) Li, H.; Wu, H. Z.; Shi, J. L. *J. Alloy. Compd.* **2013**, *556*, 71-78.
(18) Groen, J. C.; Moulijn, J. A.; Perez-Ramirez, J. *J. Mater. Chem.* **2006**, *16*, 2121-2131.
(19) Wei, X. T.; Smirniotis, P. G. *Microporous Mesoporous Mat.* **2006**, *97*, 97-106.
(20) Frontera, P.; Testa, F.; Aiello, R.; Candamano, S.; Nagy, J. B. *Microporous Mesoporous Mat.* **2007**, *106*, 107-114.
(21) Danilina, N.; Krumeich, F.; Castelanelli, S. A.; van Bokhoven, J. A. *J. Phys. Chem. C* **2010**, *114*, 6640-6645.
(22) Groen, J. C.; Jansen, J. C.; Moulijn, J. A.; Perez-Ramirez, J. *J. Phys. Chem. B* **2004**, *108*, 13062-13065.
(23) Groen, J. C.; Bach, T.; Ziese, U.; Donk, A.; de Jong, K. P.; Moulijn, J. A.; Perez-Ramirez, J. *J. Am. Chem. Soc.* **2005**, *127*, 10792-10793.
(24) Groen, J. C.; Peffer, L. A. A.; Moulijn, J. A.; Perez-Ramirez, J. *Chem.-Eur. J.* **2005**, *11*, 4983-4994.
(25) Ren, N.; Bronic, J.; Jelic, T. A.; Palcic, A.; Subotic, B. *Cryst. Growth Des.* **2012**, *12*, 1736-1745.
(26) Groen, J. C.; Sano, T.; Moulijn, J. A.; Perez-Ramirez, J. *J. Catal.* **2007**, *251*, 21-27.
(27) Groen, J. C.; Zhu, W. D.; Brouwer, S.; Huynink, S. J.; Kapteijn, F.; Moulijn, J. A.; Perez-Ramirez, J. *J. Am. Chem. Soc.* **2007**, *129*, 355-360.
(28) Mei, C. S.; Liu, Z. C.; Wen, P. Y.; Xie, Z. K.; Hua, W. M.; Gao, Z. *J. Mater. Chem.* **2008**, *18*, 3496-3500.
(29) Mei, C. S.; Wen, P. Y.; Liu, Z. C.; Liu, H. X.; Wang, Y. D.; Yang, W. M.; Xie, Z. K.; Hua, W. M.; Gao, Z. *J. Catal.* **2008**, *258*, 243-249.
(30) Perez-Ramirez, J.; Abello, S.; Villaescusa, L. A.; Bonilla, A. *Angew. Chem.-Int. Edit.* **2008**, *47*, 7913-7917.
(31) Perez-Ramirez, J.; Abello, S.; Bonilla, A.; Groen, J. C. *Adv. Funct. Mater.* **2009**, *19*, 164-172.

(32) de Jong, K. P.; Zecevic, J.; Friedrich, H.; de Jongh, P. E.; Bulut, M.; van Donk, S.; Kenmogne, R.; Finiels, A.; Hulea, V.; Fajula, F. *Angew. Chem.-Int. Edit.* **2010**, *49*, 10074-10078.
(33) Verboekend, D.; Vile, G.; Perez-Ramirez, J. *Adv. Funct. Mater.* **2012**, *22*, 916-928.
(34) Dybowski, C.; Bai, S.; Van Bramer, S. *Anal. Chem.* **2002**, *74*, 2713-2718.
(35) Jiang, Y. J.; Huang, J.; Dai, W. L.; Hunger, M. *Solid State Nucl. Magn. Reson.* **2011**, *39*, 116-141.
(36) Koller, H.; Weiss, M. *Solid State NMR of Porous Materials* **2012**, *306*, 189-227.
(37) Li, S. H.; Deng, F. *Annual Reports on Nmr Spectroscopy* **2013**, *78*, 1-54.
(38) Cadars, S.; Lesage, A.; Hedin, N.; Chmelka, B. F.; Emsley, L. *J. Phys. Chem. B* **2006**, *110*, 16982-16991.
(39) Morais, C. M.; Montouillout, V.; Deschamps, M.; Iuga, D.; Fayon, F.; Paz, F. A. A.; Rocha, J.; Fernandez, C.; Massiot, D. *Magn. Reson. Chem.* **2009**, *47*, 942-947.
(40) Delevoye, L.; Fernandez, C.; Morais, C. M.; Amoureux, J. P.; Montouillout, V.; Rocha, J. *Solid State Nucl. Magn. Reson.* **2002**, *22*, 501-512.
(41) Lutz, W.; Wieker, W.; Muller, D.; Schneider, M.; Ruscher, C. H.; Buhl, J. C. *Z. Anorg. Allg. Chem.* **2000**, *626*, 1460-1467.
(42) Lutz, W.; Bertram, R.; Heidemann, D.; Kurzhals, R.; Ruscher, C.; Kryukova, G. *Z. Anorg. Allg. Chem.* **2011**, *637*, 75-82.
(43) Qin, Z. X.; Shen, B. J.; Yu, Z. W.; Deng, F.; Zhao, L.; Zhou, S. G.; Yuan, D. L.; Gao, X. H.; Wang, B. J.; Zhao, H. J.; Liu, H. H. *J. Catal.* **2013**, *298*, 102-111.
(44) Calsavara, V.; SousaAguiar, E. F.; Machado, N. *Zeolites* **1996**, *17*, 340-345.
(45) Liu, D. S.; Bao, S. L.; Xu, Q. H. *Zeolites* **1997**, *18*, 162-170.
(46) Philippaerts, A.; Goossens, S.; Vermandel, W.; Tromp, M.; Turner, S.; Geboers, J.; Van Tendeloo, G.; Jacobs, P. A.; Sels, B. F. *ChemSusChem* **2011**, *4*, 757-767.
(47) Philippaerts, A.; Geboers, J.; Sels, B. F. WO 2012/068645, 2012.
(48) Medek, A.; Harwood, J. S.; Frydman, L. *J. Am. Chem. Soc.* **1995**, *117*, 12779-12787.
(49) Huang, J.; van Vegten, N.; Jiang, Y. J.; Hunger, M.; Baiker, A. *Angew. Chem.-Int. Edit.* **2010**, *49*, 7776-7781.
(50) Buchholz, A.; Wang, W.; Xu, M.; Arnold, A.; Hunger, M. *J. Phys. Chem. B* **2004**, *108*, 3107-3113.
(51) Kao, H. M.; Grey, G. P. *J. Phys. Chem.* **1996**, *100*, 5105-5117.
(52) Fyfe, C. A.; Bretherton, J. L.; Lam, L. Y. *J. Am. Chem. Soc.* **2001**, *123*, 5285-5291.
(53) Omegna, A.; van Bokhoven, J. A.; Prins, R. *J. Phys. Chem. B* **2003**, *107*, 8854-8860.

TOC

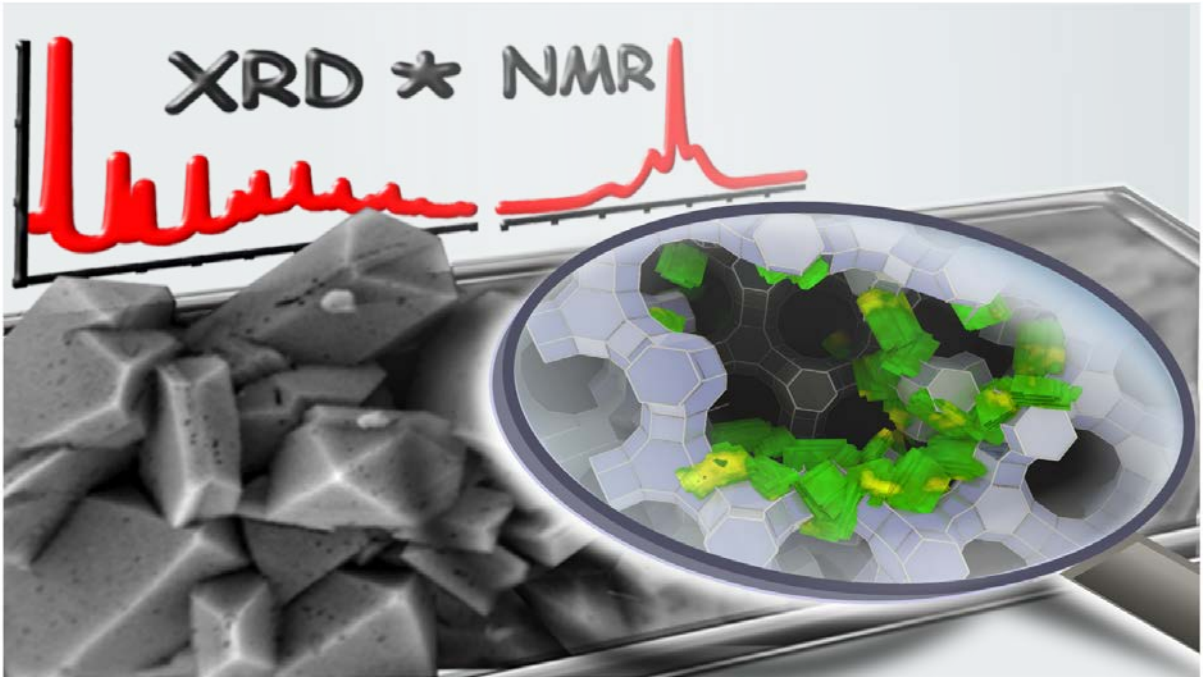

Synopsis

The structural modification of USY zeolite by NH_4OH treatment was studied in details by NMR and XRD. The aqueous ammonia treatment led to a very low level of desilication, no significant dealumination and to a progressive loss in crystallinity of the pristine zeolite. USY crystal fraction decreases with treatment time, correlated to a mesoporous volume increase. The progressive migration of silicon and aluminum atoms from zeolite into a dense phase causes a progressive partial amorphization of the material.

Supporting Information

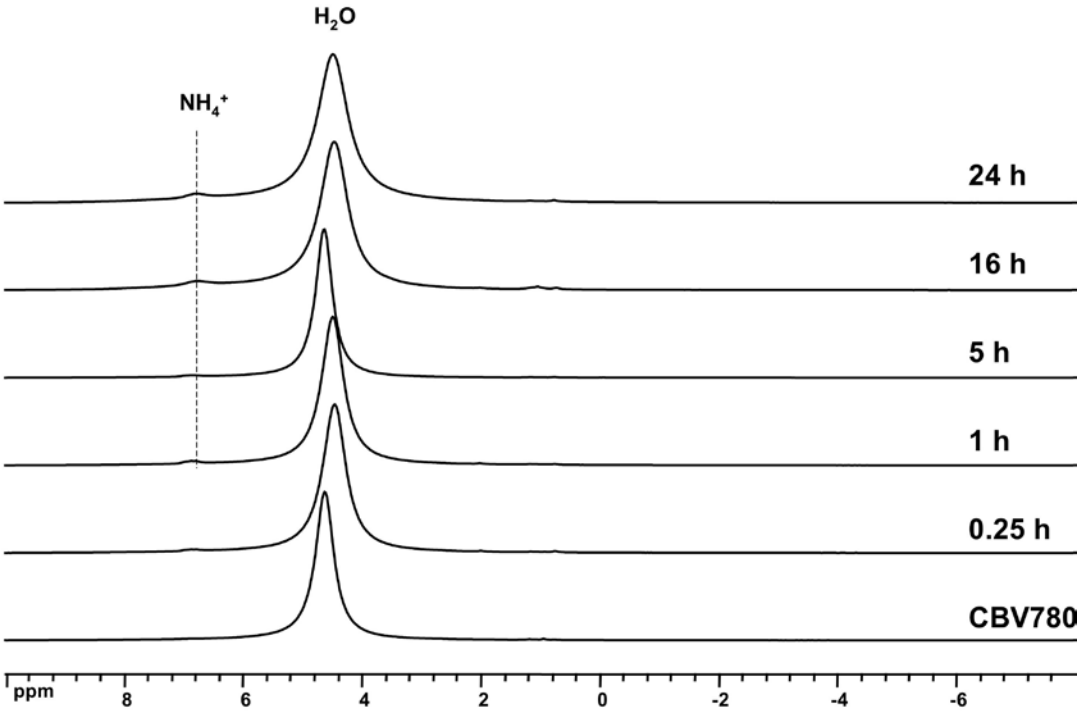

Figure S1. ^{1}H MAS NMR spectra of USY samples before and after NH_4OH treatment for different contact times and subsequently dried at 100 °C followed by calcination at 350 °C: a) pristine zeolite, b) USY(0.25)-calc, c) USY(1)-calc, d) USY(5)-calc, e) USY(16)-calc, f) USY(24)-calc.

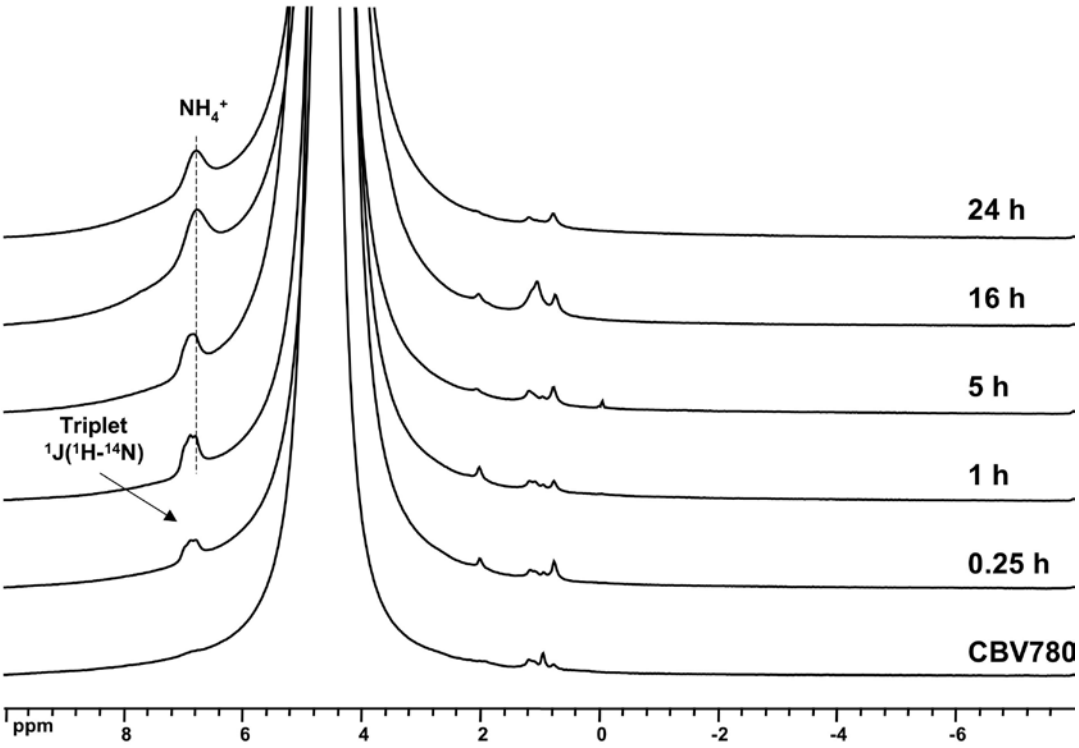

Figure S2. Vertical expansion of ^{1}H MAS NMR spectra of USY samples before and after NH_4OH treatment for different contact times and subsequently dried at 100 °C followed by calcination at 350 °C: a) pristine zeolite, b) USY(0.25)-calc, c) USY(1)-calc, d) USY(5)-calc, e) USY(16)-calc, f) USY(24)-calc.

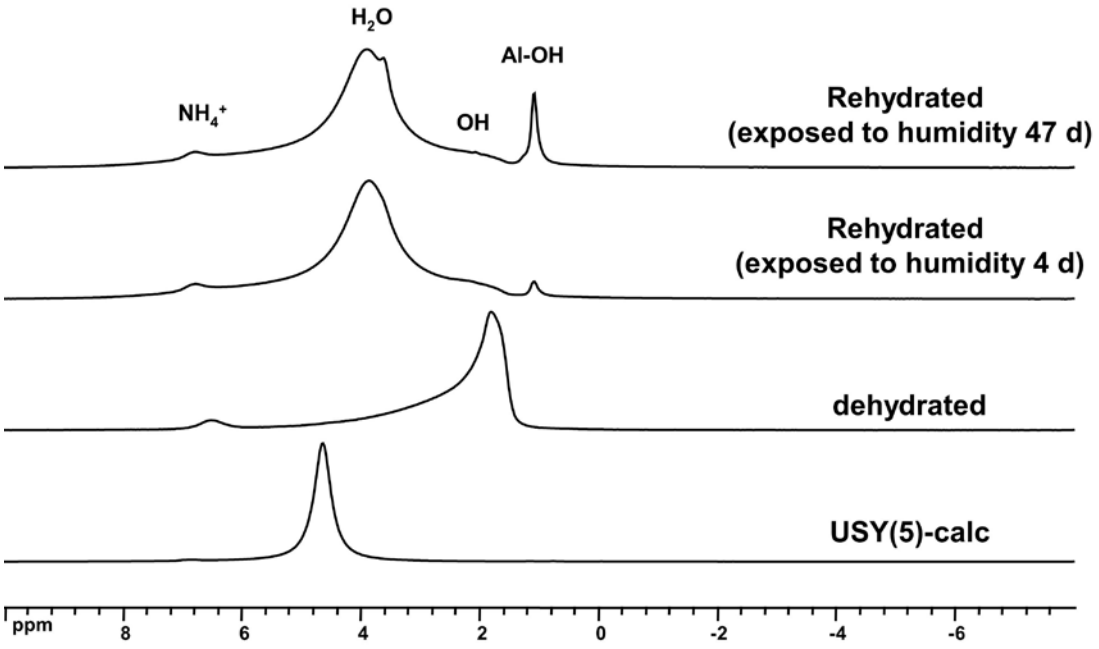

Figure S3. ^{1}H MAS NMR spectra of USY(5)-calc sample before and after dehydration, and then subsequent different stages of rehydration.

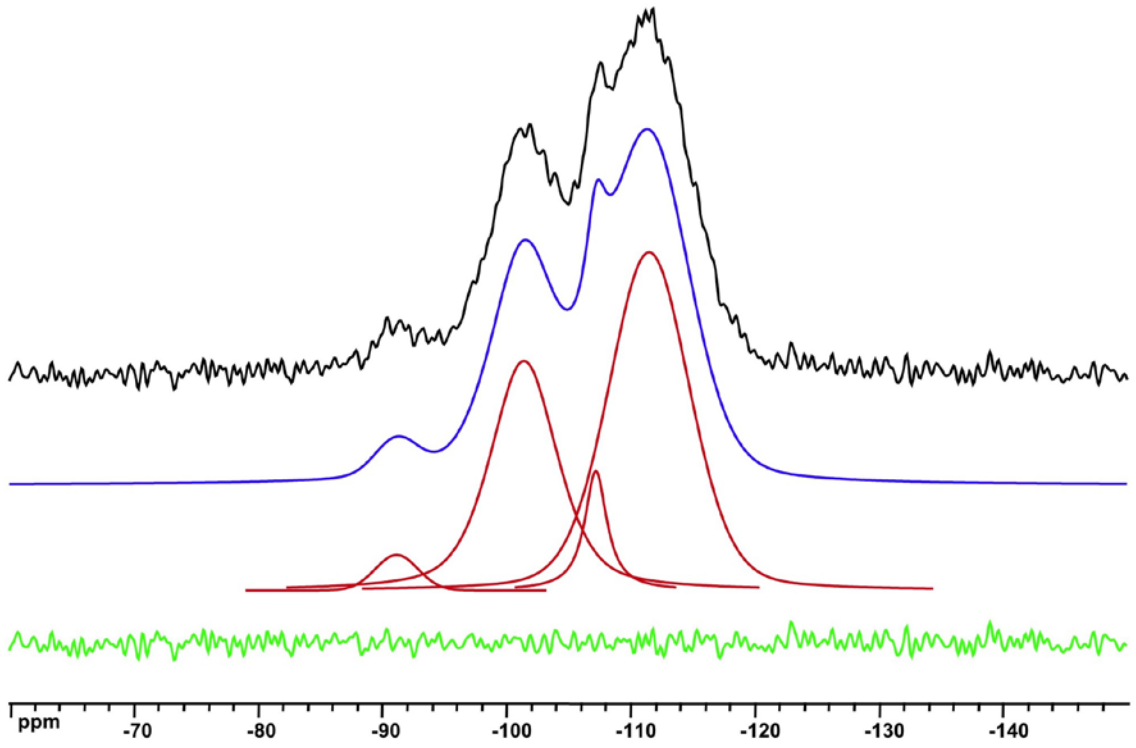

Figure S4. Example of spectral decomposition of ^{29}Si hpDec MAS NMR of USY(16)-calc spectrum: Black line (experimental), Blue line (calculated), Red lines (components), Green line (difference).

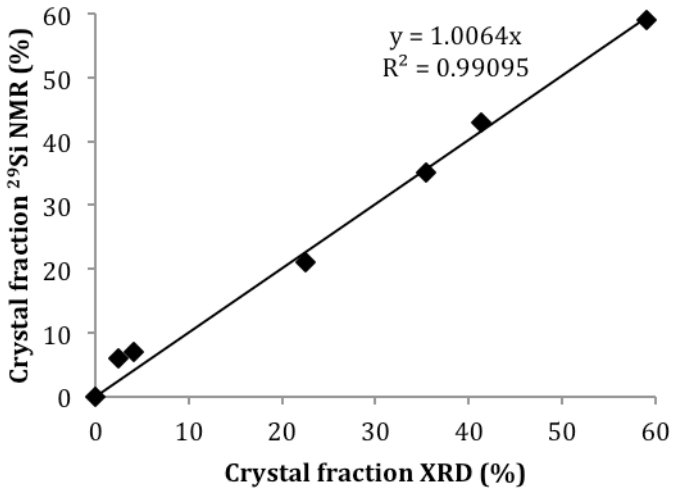

Figure S5. Correlation of the crystal fraction (periodic USY-Q^4 Si) measured by ^{29}Si single pulse with ^{1}H decoupling MAS NMR (See Table 3) with the crystal fraction obtained by XRD (See Table 1) for USY samples after treatment with NH_4OH solution for all different contact times and subsequently dried at 100 °C followed by calcination at 350 °C. XRD calibration of the parent USY has used crystalline to amorphous fractions obtained by NMR for this specific sample. With this calibration point of 59 % (pristine zeolite) the results form a series of points extrapolate consistently with the second point of calibration (0 % for USY(24)-RT) exhibiting a fairly good alignment onto to y = x correlation curve.

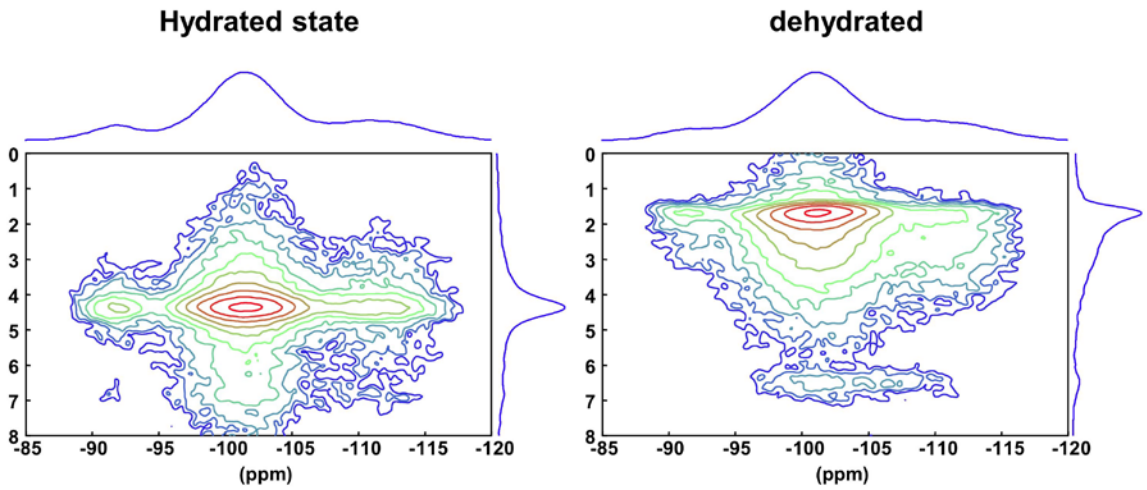

Figure S6. $^{1}H \rightarrow {}^{29}Si$ CPHETCOR MAS NMR of USY(16)-calc in a) hydrated state, and b) after dehydration.

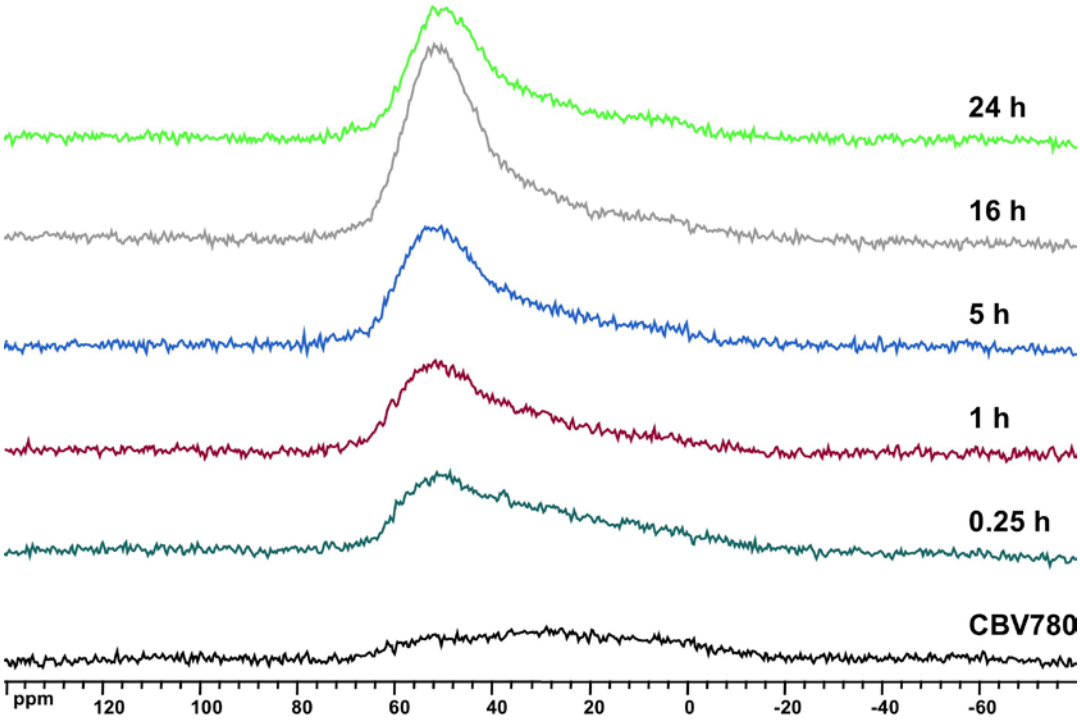

Figure S7. Stack plot of ^{27}Al MAS NMR spectra of USY samples in dehydrated state before and after NH_4OH treatment for different contact times and subsequently dried at 100 °C followed by calcination at 350 °C: a) pristine zeolite, b) USY(0.25)-calc, c) USY(1)-calc, d) USY(5)-calc, e) USY(16)-calc, f) USY(24)-calc.

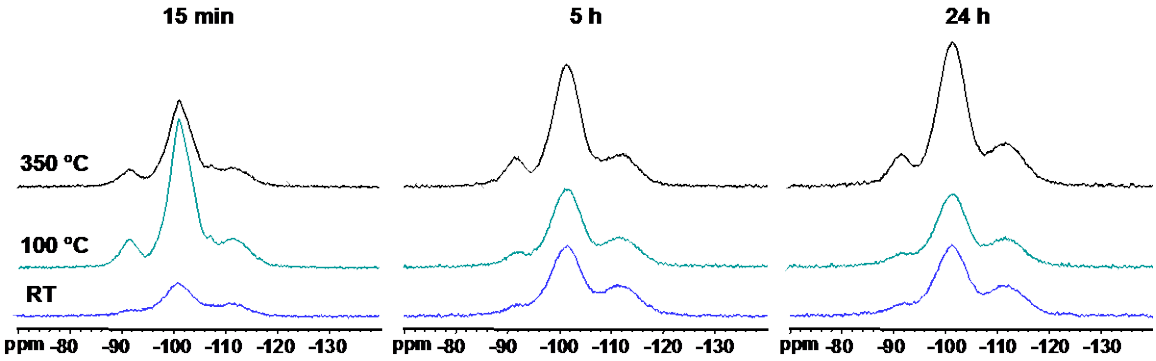

Figure S8. ^{29}Si CPMAS NMR spectra of USY samples after NH_4OH treatment for 0.25, 5, and 24 h and subsequently, dried at room temperature (USY(0.25)-RT, USY(5)-RT, and USY(24)-RT), dried at 100 °C (USY(0.25)-100°C , USY(5)-100°C , and USY(24)-100°C), and dried at 100 °C followed by calcination at 350 °C (USY(0.25)-calc, USY(5)-calc, and USY(24)-calc).

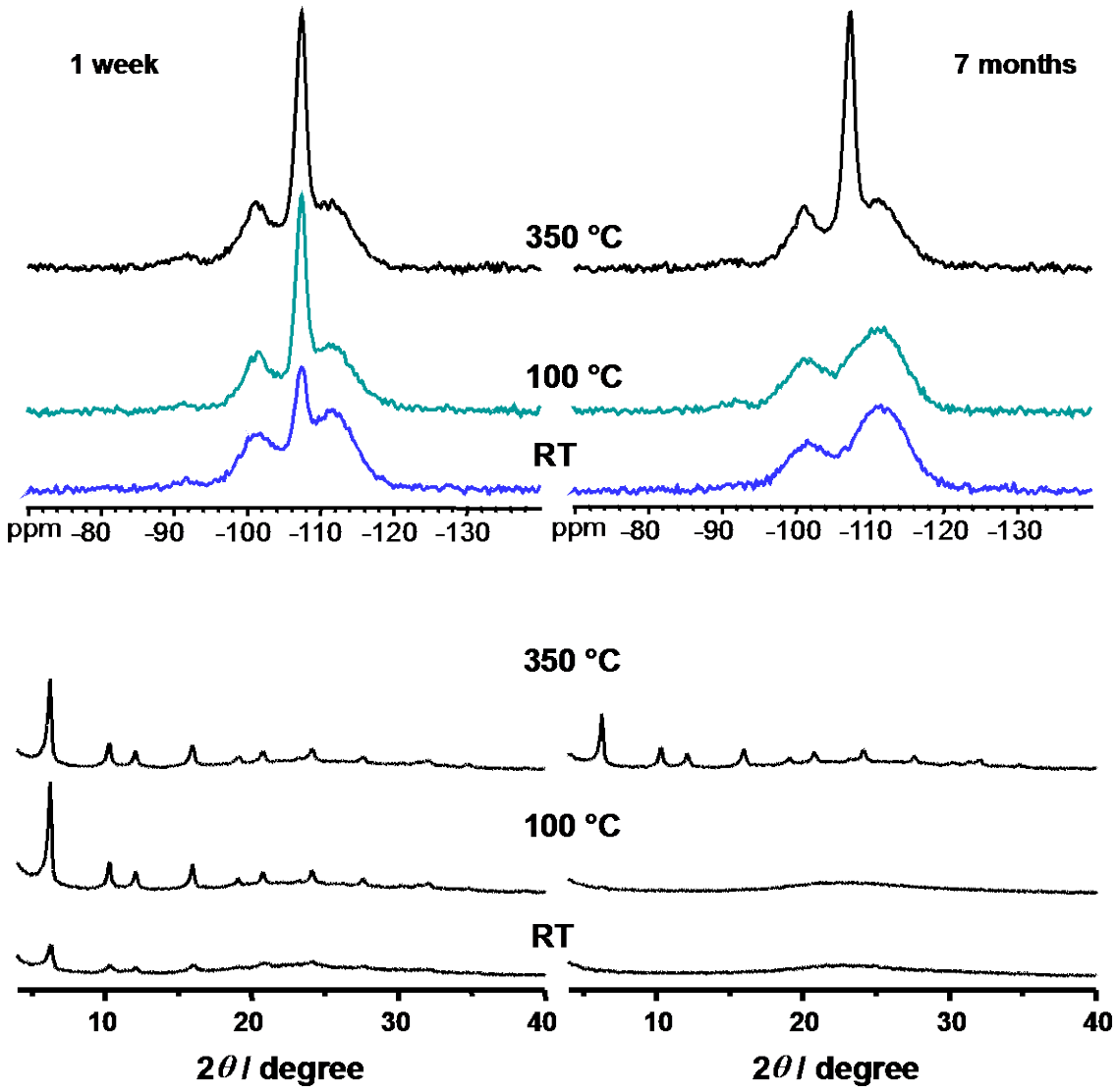

Figure S9. Evolution with time of ^{29}Si MAS NMR spectra (top) and XRD patterns (bottom) of USY samples after NH_4OH treatment for 0.25 h and subsequently, dried at room temperature, dried at 100 °C, and dried at 100 °C followed by calcination at 350 °C.

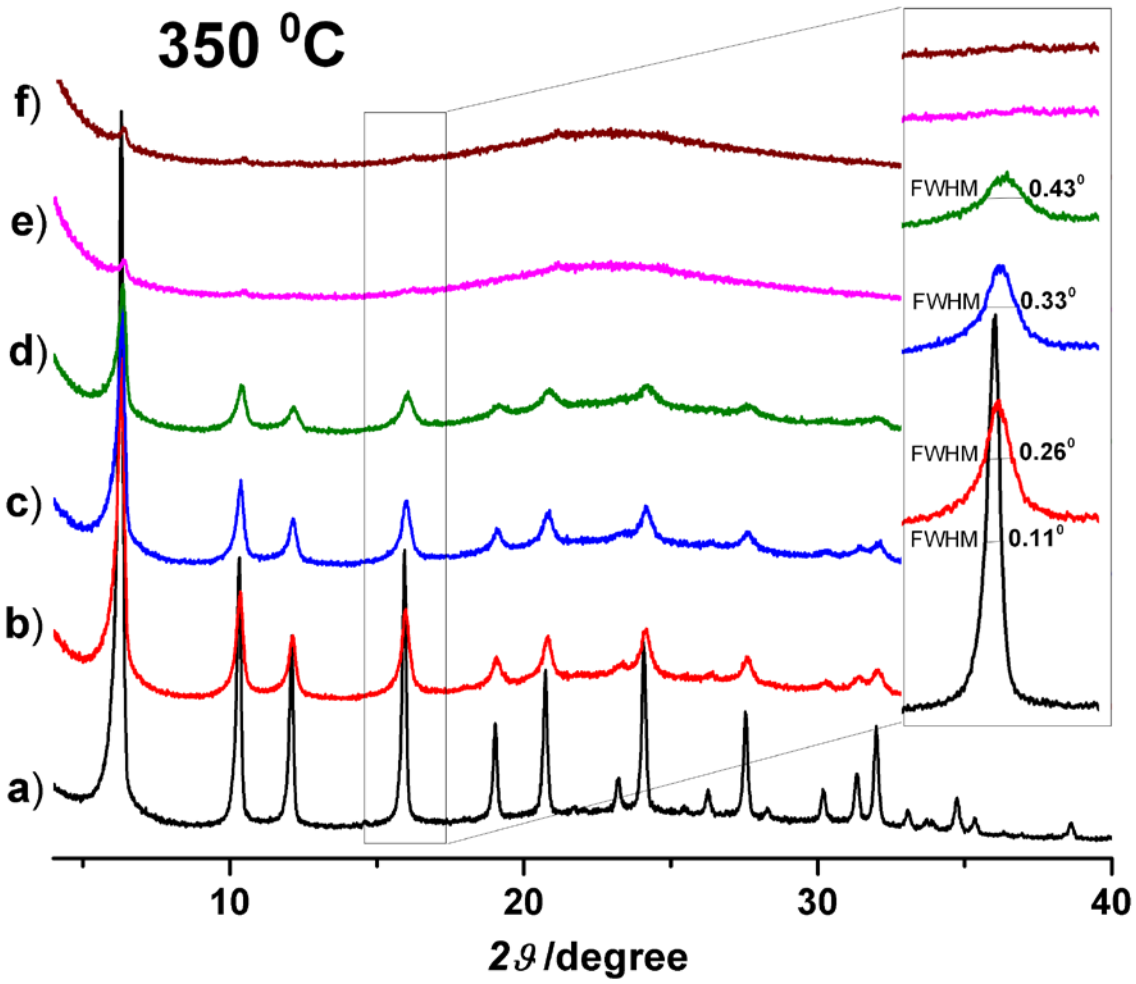
350 ^{0}C
f)
e)
d)
c)
b)
a)
FWHM 0.43^0
FWHM 0.33^0
FWHM 0.26^0
FWHM 0.11^0
10
20
30
40
2ϑ /degree

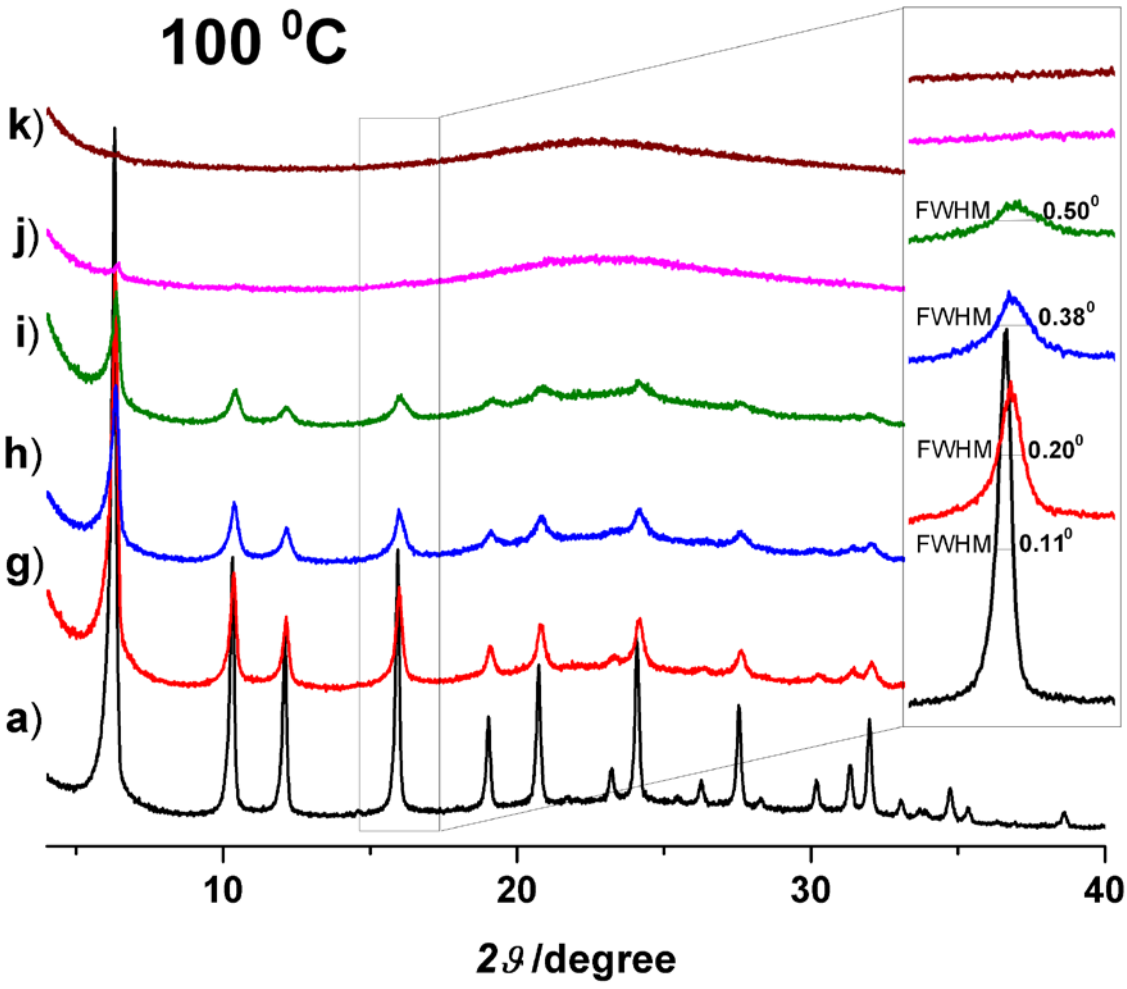
100 °C
k)
j)
i)
h)
g)
a)
FWHM 0.50°
FWHM 0.38°
FWHM 0.20°
FWHM 0.11°
10
20
30
40
2ϑ /degree

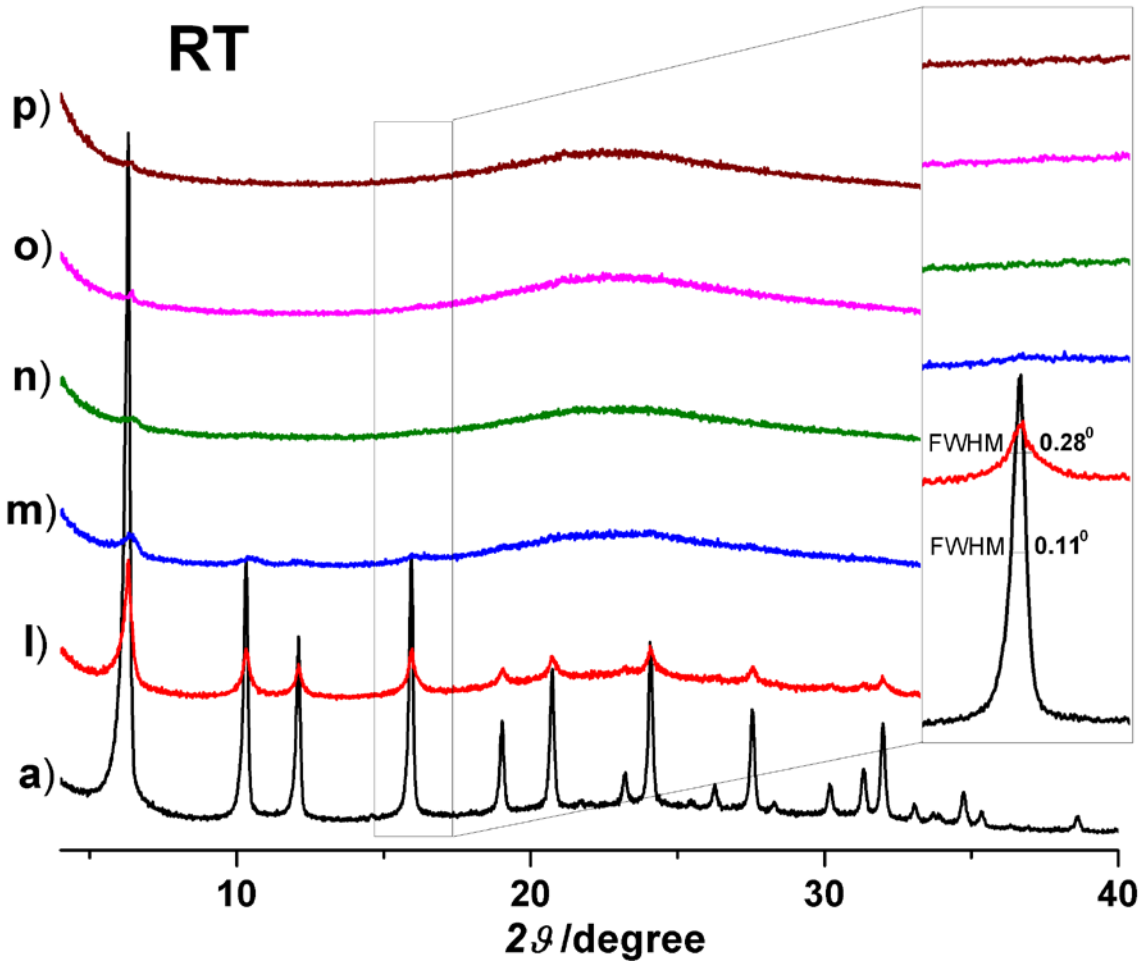

Figure S10:

XRD patterns of USY samples before (a) and after NH_4OH treatment at different contact times and subsequently either dried at 100 °C followed by calcination at 350 °C (b-f): a) pristine zeolite, b) USY(0.25)-calc, c) USY(1)-calc, d) USY(5)-calc, e) USY(16)-calc, f) USY(24)-calc; 100°C dried (g-k): a) pristine zeolite, g) USY(0.25)-100°C , h) USY(1)-100°C , i) USY(5)-100°C , j) USY(16)-100°C , k) USY(24)-100°C ; dried at room temperature (l-p): a) pristine zeolite, l) USY(0.25)-RT, m) USY(1)-RT, n) USY(5)-RT, o) USY(16)-RT, p) USY(24)-RT.